Analytical Methods

PAPER

View Article Online
View Journal | View Issue

Cite this: *Anal. Methods*, 2015, **7**, 3903

A highly sensitive electrochemical OP biosensor based on electrodeposition of Au–Pd bimetallic nanoparticles onto a functionalized graphene modified glassy carbon electrode

Haijun Zhan, Jie Li, Zhimin Liu,* Yingying Zheng and Yanfeng Jing

Received 16th March 2015
Accepted 31st March 2015

DOI: 10.1039/c5ay00702j

www.rsc.org/methods

A fast and stable organophosphate pesticide (OP) biosensor with enhanced sensitivity has been developed for the detection of OPs by using Au–Pd bimetallic nanoparticles and ionic liquid functionalized graphene–chitosan nanocomposites (Au–Pd/IL-GR–CHI). An electrodeposition method was first applied to form Au–Pd nanoparticles on the surface of IL-GR–CHI, which were characterized by scanning electron microscopy and electrochemical methods. The electron transfer resistance of the Au–Pd/IL-GR–CHI modified electrode was smaller than that of the Au/IL-GR–CHI (or Pd/IL-GR–CHI) modified electrode, indicating that the presence of Au–Pd/IL-GR–CHI hybrid nanocomposites on the electrode surface could improve the reactive sites, reduce the interfacial resistance, and make the electron transfer easier. The Au–Pd/IL-GR–CHI hybrid nanocomposites with excellent conductivity, catalytic activity and biocompatibility offered an extremely hydrophilic surface for AChE adhesion. Under optimal conditions, based on the inhibition of organophosphate pesticides (OPs) on the AChE activity, using phorate as a model compound, the biosensor detected phorate in the linear range from 5.0×10^{-16} to 2.5×10^{-13} M and from 4.9×10^{-13} to 9.5×10^{-6} M, with a detection limit of 2.5×10^{-16} M ($S/N = 3$). The developed biosensor exhibited many advantages such as high sensitivity, acceptable stability and low cost, thus providing a promising tool for the analysis of OPs.

1. Introduction

Highly sensitive detection of organophosphorus pesticides (OPs) has attracted increasing attention in the past couple of decades due to their high toxicity and persistence. To this aim, different detection technologies were developed.[1–4] Among them, electrochemical biosensors based on the inhibition of acetylcholinesterase (AChE) are regarded as highly promising candidates for OP detection because of their advantages of rapidity, simplicity and economy.[5–7] These devices are designed to complement or replace the existing analytical methods such as GC and GC/MS by simplifying sample preparation, thus decreasing the analysis time and cost. However, so far, the detection limits of AChE biosensors have not been able to reach the same level as those of analysis instruments. Herein, we are looking for a way to develop a better AChE electrochemical biosensor with high sensitivity and selectivity. Therefore, the selection of materials becomes critical.

In the past few years, graphene (GR) has captured great interest among scientists owing to its high surface area, excellent electrical conductivity and low cost.[8,9] Because of its interesting physical properties, graphene shows excellent application potential in nanoelectronic devices and sensors.[10,11] Recently, the electrochemical biosensing applications of GR and GR-based hybrid nanomaterials have been explored.[12–16] However, due to the existence of strong van der Waals interactions among the reduced graphene sheets, graphene sheets easily form irreversible agglomerates in solutions.[17] Therefore, chemical modifications or non-covalent functionalizations have been used to improve the solvency of GR. Ionic liquids (ILs) are green solvents that are composed entirely of cations and anions, which have aroused tremendous interest in chemical research. Considerable results demonstrated that ILs could be the superior solvents for the synthesis of nanostructured materials because of their unique characteristics, such as wide electrochemical window, excellent conductivity and high chemical stability.[18,19] It has been found recently that ILs with imidazolium cations can interact with GR through π–π stacking and serve as a stabilizer to effectively prevent the aggregation of graphene sheets.[20,21] In addition, other related reports found in the literature substantiated that the use of IL functionalized graphene sheets (IL-GR) could increase the sensitivity of the response and facilitate efficient electron transfer of various redox biomolecules.[22] Thus, IL-GR nanocomposites are

College of Chemistry and Chemical Engineering, Henan University of Technology, 100 North Zhongyuan Road, Zhengzhou 450001, China. E-mail: zhimin@haut.edu.cn; Fax: +86-371-67756718; Tel: +86-371-67756718

expected to be useful and powerful materials for enhancing the electrochemical performance for the detection of different target molecules in electroanalytical applications.

Recently, GR-based hybrid nanomaterials with metallic nanoparticles have shown potential applications in the area of chemical sensors, energy storage and catalysis.[23,24] GR-based hybrids with metallic composite materials could provide larger electrochemically active surface areas for the adsorption of enzymes and effectively accelerate the electron transfer between the electrode and detection molecules.[25] For example, the Dong group successfully synthesized graphene/platinum hybrid nanostructures by alternatively assembling ionic liquid-modified graphene nanosheets and platinum nanoparticles.[26] The obtained hybrid nanomaterials exhibited good electrochemical properties. Cao and his colleague successfully synthesized platinum–palladium–chitosan–graphene hybrid nanocomposites (PtPd–CS–GS) for the construction of a cholesterol biosensor. The PtPd–CS–GS nanocomposites showed a significant increase of electronic conductivity.[27] Moreover, other related reports indicated that some graphene-supported bimetallic nanoparticles, such as Au–Pd/GR and Pd–Ru/GR,[28,29] could exhibit excellent catalytic performance in various reactions. For instance, Wang *et al.* studied the catalytic activity of graphene supported Au–Pd bimetallic nanoparticles in methanol selective oxidation to methyl formate, and the results showed that the catalytic performance was excellent.[28] Considering the advantageous properties of IL-GR and bimetallic nanoparticles, in the present work, we tried to combine IL-GR with Au–Pd bimetallic nanoparticles for the preparation of the electrochemical AChE biosensor.

Chitosan (CHI) is an abundant natural biopolymer. It has been universally used as an immobilization matrix for biofabrication due to its good water permeability, excellent film forming ability, good biocompatibility and high mechanical strength.[30] Moreover, some literature reported that CHI could accumulate metal ions through various mechanisms, such as electrostatic attraction, ion exchange and chelation.[31,32] So in this study, CHI was combined to IL-GR to form a homogeneous IL-GR–CHI suspension. Herein, CHI not only acts as an effective solubilizing agent for dispersing IL-GR, which can have a good film-forming ability on the electrode surface, but also as a polymer for accumulating Au–Pd bimetallic nanoparticles to obtain a nanostructural Au–Pd/IL-GR–CHI composite membrane with the further enhancement of surface area and electron transfer rate.

Accordingly, in this work, a highly sensitive AChE biosensor based on the Au–Pd/IL-GR–CHI composite membrane has been developed. Firstly, the IL-GR–CHI nanocomposite film was assembled on the surface of the glassy carbon electrode (GCE). Secondly, Au–Pd bimetallic nanoparticles were electrodeposited on the IL-GR–CHI/GCE. Finally, AChE was immobilized onto the nanocomposites to obtain an AChE biosensor for the detection of OPs. The biosensor has been demonstrated to be a device with high sensitivity, acceptable stability and reproducibility for the analysis of phorate. Therefore, the present work offers a new avenue to broaden the applications of graphene in electrochemical biosensors.

2. Experimental

2.1. Reagents and materials

Acetylthiocholine chloride (ATCl) and AChE (Type C 3389, 500 U mg^{-1} from an electric eel) were purchased from Sigma-Aldrich (St. Louis, USA). Chitosan (CHI), $PdCl_2$ and $HAuCl_4$ were obtained from Sinopharm Chemical Reagent Co., Ltd. (Shanghai, China). Phorate (99.8%) was provided by Beijing Putian Tongchuang Biotechnology Co. Ltd. (Beijing, China). Phosphate buffer solutions (PBS) with different pH values were prepared by mixing 0.1 M Na_2HPO_4 and 0.1 M KH_2PO_4. Distilled water was used throughout this study. All other chemicals were of analytical grade and used as received without further purification.

Electrochemical measurements were carried out with a CHI 660E electrochemical analyzer (Shanghai CH Instrument Company, Shanghai, China). A conventional three-electrode system was employed with a saturated calomel electrode (SCE) as the reference electrode, a platinum foil as the counter electrode, and the modified GCE (3 mm diameter) as the working electrode. Scanning Electron Microscopy (SEM) measurement was carried out using a JSM-7500F for surface morphology observations. X-ray diffraction (XRD) patterns were obtained using an Ultima IV diffractometer. All the measurements were carried out at room temperature.

2.2. Synthesis of ionic liquid functionalized graphene (IL-GR)

Ionic liquid 1-(3-aminopropyl)-3-methylimidazolium bromide (IL-NH_2) was prepared following the reported work with slight modification.[33] Under a nitrogen atmosphere, 1-methylimidazole (4.56 mmol) and 3-bromopropylamine hydrochloride (4.56 mmol) were dissolved into 50 ml of anhydrous ethanol under stirring. The resulting mixture was refluxed at 65 °C under nitrogen protection for 24 h. After removal of ethanol in a vacuum, the solid residue was dissolved into water. Then the pH value of the solution was adjusted to pH 10.0 by the addition of potassium hydroxide. The obtained solution was concentrated under vacuum and then extracted with ethanol–tetrahydrofuran (V/V, 1 : 1). The resulting 1-(3-aminopropyl)-3-methylimidazolium bromide (IL-NH_2) was dried at 60 °C overnight.

Graphite oxide (GO) was prepared from graphite powder by the modified Hummers method. Ionic liquid functionalized graphene (IL-GR) was synthesized by an epoxide ring-opening reaction between GO and 1-(3-aminopropyl)-3-methylimidazolium bromide (IL-NH_2) according to the literature.[34]

2.3. Fabrication of the proposed biosensor

Prior to the surface modification, the GCE was polished with 0.3 and 0.05 μm alumina slurry to obtain a mirror-like surface and sequentially sonicated in ethanol and water.

1.0 mg of IL-GR was added to 1.0 ml of 0.5% CHI (Wt/V, 50 mM acetic acid) solution and sonicated thoroughly until a homogeneous suspension of IL-GR–CHI was obtained, then 5 μl of the suspension was coated on the cleaned electrode to prepare the IL-GR–CHI/GCE, and the modified electrode was left to dry at room temperature.

Subsequently, the electrochemical deposition of Au–Pd nanoparticles onto the IL-GR–CHI/GCE was carried out in 0.25% CHI solution containing 2.5 mM $HAuCl_4$ and 2.5 mM $PdCl_2$. The deposition time was 80 s and the potential was −1.0 V. After that, the modified electrode was gently washed with water and dried in air. The obtained electrode was denoted as the Au–Pd/IL-GR–CHI/GCE. Ultimately, AChE solution was mixed with 0.5% CHI solution (V/V, 1 : 1), 5 μl of the resulting solution was cast onto the Au–Pd/IL-GR–CHI/GCE surface using a syringe, and the modified electrode (noted as AChE/Au–Pd/IL-GR–CHI/GCE) was moved into a refrigerator and kept at 4 °C to dry overnight. The preparation process of the modified AChE/Au–Pd/IL-GR–CHI/GCE is shown in Scheme 1.

2.4. Measurement procedure

The prepared AChE/Au–Pd/IL-GR–CHI/GCE was first activated in pH 6.5 PBS by cyclic voltammetric sweeps from −0.2 to 0.8 V until stable curves were obtained. For the measurement of phorate, the pretreated AChE/Au–Pd/IL-GR–CHI/GCE was first immersed in the PBS solution containing different concentrations of standard organophosphate pesticides for 6 min, and then transferred to the electrochemical cell of 10 ml pH 6.5 PBS containing 1.0 mM ATCl to study the electrochemical response by differential pulse voltammetry.

The apparent Michaelis–Menten constant (K_m^{app}) of the biosensor, which gives an indication of the enzyme substrate kinetics for the biosensor, was determined by the analysis of the slope and intercept of the plot of the reciprocals of the steady-state current *versus* ATCl concentration.

2.5. Analysis of phorate in spiked apple juice samples

The apple juice was purchased from a local supermarket in China. The pH of juices was adjusted to ~6.5 by 0.1 M NaOH. Several phorate standard solutions were mixed into the apple juice samples to obtain final concentrations of 0.0005, 0.005, 0.1, 50 and 100 nM. The apple juice samples were filtered through a 0.22 μm filter[35] and the filtrates were tested using the as-prepared AChE/Au–Pd/IL-GR–CHI/GCE biosensor.

3. Results and discussion

3.1. Characterization

Fig. 1(A) shows XRD patterns of Au–Pd/IL-GR (curve a) and GO (curve b). The diffraction peaks of Au–Pd/IL-GR at 38.4°, 44.5°, 64.7° and 78.2° were assigned to the (1 1 1), (2 0 0), (2 2 0) and (3 1 1) crystal planes of the Au and/or Pd, respectively. The diffraction peaks slightly shifted and fell in between those of bulk Au (JCPDS no. 04-0784) and Pd (JCPDS no. 46-1043) in the standard XRD patterns, showing the formation of the single-phase Au–Pd bimetallic nanoparticles.[36] Additionally, an extra broad peak emerged at 23° for Au–Pd/IL-GR (curve a), different from GO only with a sharp peak centered at 11° (curve b), owing to the removal of oxygen-containing functional groups from GO, strongly manifesting the efficient reduction of GO.

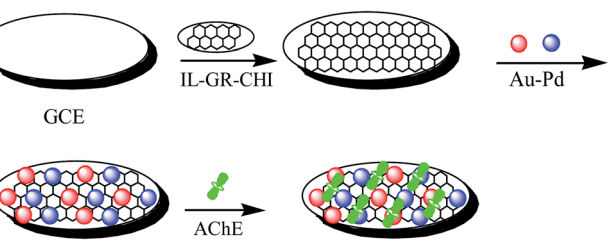

Scheme 1 The schematic diagram of the fabrication of the OP biosensor.

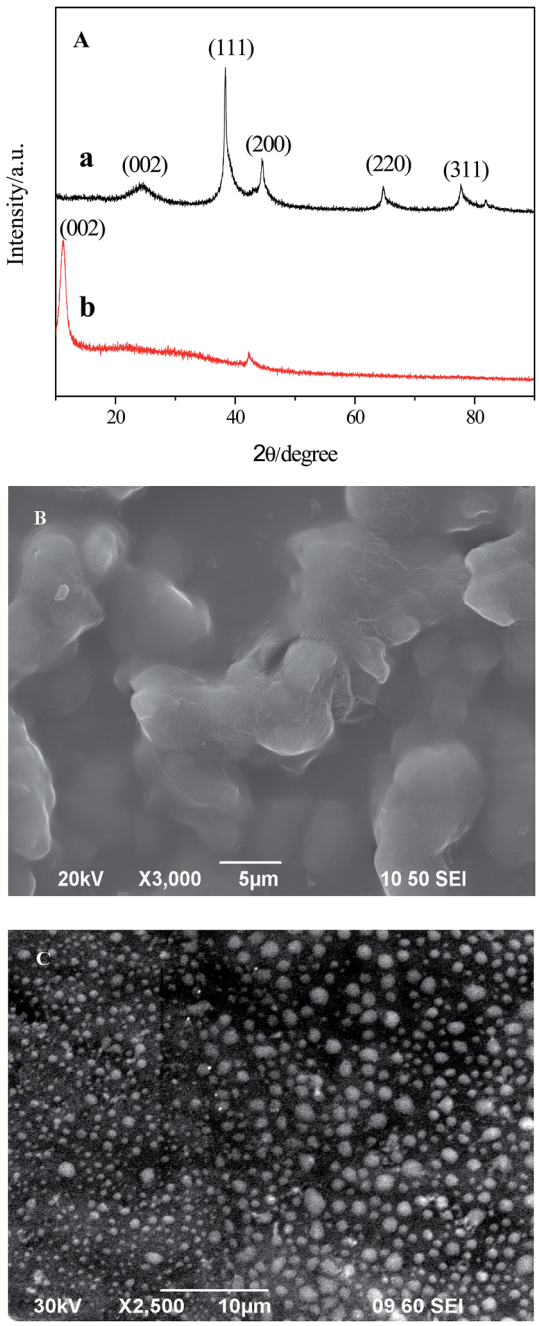

Fig. 1 (A) XRD patterns of Au–Pd/IL-GR (curve a) and GO (curve b); SEM images of IL-GR–CHI/GCE (B) and Au–Pd/IL-GR–CHI/GCE (C).

The surface morphology of different electrodes was investigated by SEM observation. Fig. 1(B) displays the surface morphology of the IL-GR–CHI/GCE. It can be seen that a few layer crumpled sheets of IL-GR were formed on the surface of the GCE. Then the Au–Pd nano-particles appeared as bright dots, which occupied almost all of the surfaces of IL-GR–CHI with fairly even, ordered and close-packed distribution as in Fig. 1(C), forming an interpenetrating network for favorable conduction pathways of electron transfer. The average diameter of the formed randomly dot structures varied from tens to hundreds of nanometers.

3.2. Electrochemical impedance spectroscopy of different electrodes

Electrochemical impedance spectroscopy (EIS) is a well-known effective method for studying the interface properties, which can give information about the stepwise assembly of the biosensor based on the impedance changes of the electrode surface. In a typical EIS plot, the diameter of the semicircular portion is equal to the electron transfer resistance (R_{et}) in a higher frequency range. The obtained Nyquist plots are presented in Fig. 2A and the equivalent electrical circuit used to fit the electrochemical impedance data is presented in Fig. 2B. According to the standard complex function representation, the impedance data can be described as a real $Z'(\omega)$ and an imaginary part $Z''(\omega)$ (eqn (1) and (2)):[37]

$$Z'(\omega) = R_s + R_{et}\,(1 + \omega^2 \times {C_{dl}}^2 \times {R_{et}}^2)^{-1} \quad (1)$$

$$-Z''(\omega) = \omega \times C_{dl} \times {R_{et}}^2 \times (1 + \omega^2 \times {C_{dl}}^2 \times {R_{et}}^2)^{-1} \quad (2)$$

where R_s/Ω is the resistance of the electrolyte; R_{et}/Ω is the electron transfer resistance; C_{dl}/F is the double-layer capacitance of the system and ω is the angular frequency ($\omega = 2 \times \pi \times f$; f is the ac-frequency).[37]

According to the equivalent model circuit, the observed R_{et} value was 287.2 Ω for the bare GCE (curve a). After the GCE was modified with IL-GR–CHI, the R_{et} value decreased sharply ($R_{et} = 188.5$ Ω, curve b), suggesting that the IL-GR layer promoted the redox probe to diffuse toward the electrode surface due to the inherent conductivity of IL-GR. When Au–Pd nanoparticles were deposited on the IL-GR–CHI membrane (curve c), it can be seen that the R_{et} value (122.4 Ω) of the Au–Pd/IL-GR–CHI/GCE electrode was smaller than that of the IL-GR–CHI/GCE electrode, which indicated that the presence of Au–Pd nanoparticles on the electrode surface could play an important role similar to the electron conducting tunnel, which made the electron transfer easier to take place. After AChE was successively loaded onto the electrode surface, the R_{et} value increased due to the formation of a hydrophobic protein layer which insulated the conductive support and the interfacial electron transfer (curve d).

3.3. Electrochemical behavior of different electrodes

CVs of ATCl and enzymatic product thiocholine were investigated on five different biosensors. As shown in Fig. 3, no amperometric response could be observed at the GCE (curve a)

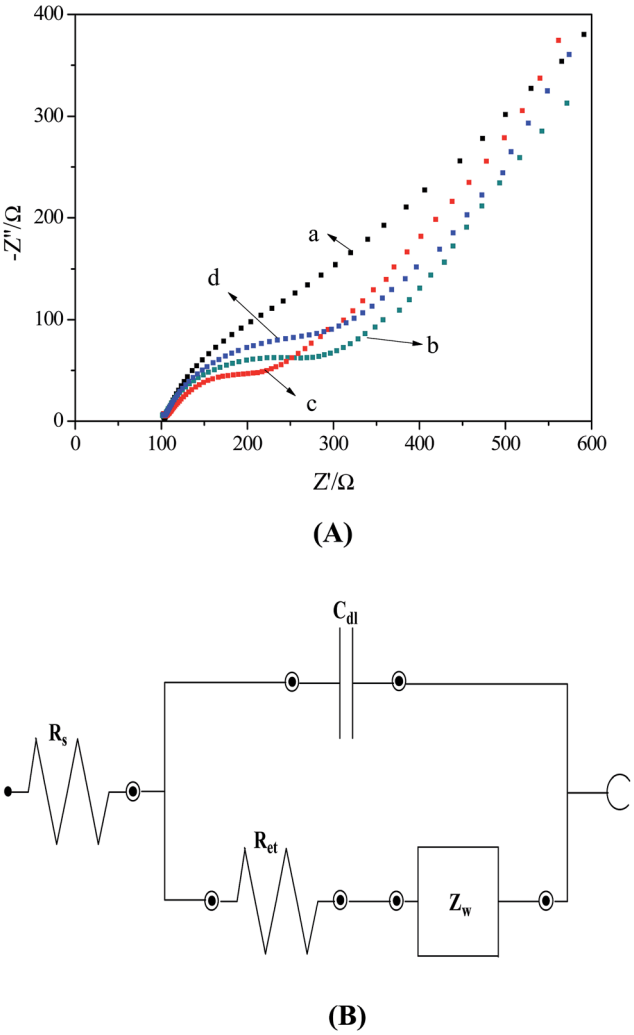

Fig. 2 (A) Electrochemical impedance spectroscopy spectra of a bare GCE (a), IL-GR–CHI/GCE (b), Au–Pd/IL-GR–CHI/GCE (c) and AChE/Au–Pd/IL-GR–CHI/GCE (d) in 5.0 mM $[Fe(CN)_6]^{3-/4-}$ containing 0.1 M KCl. (B) Equivalent electrical circuit comprising the resistance of the electrolyte (R_s/Ω), the electron transfer resistance (R_{et}/Ω), the Warburg impedance (Z_w/Ω), and the double-layer capacitance (C_{dl}/F).

and the AChE/Au–Pd/IL-GR–CHI/GCE (curve b) in 0.1 M PBS (pH 6.5). However, when 1.0 mM ATCl was added into the PBS (pH 6.5), an obvious amperometric response was observed at the AChE/Au–Pd/IL-GR–CHI/GCE (curve e), meanwhile no amperometric response could be observed at the Au–Pd/IL-GR–CHI/GCE (curve c). Obviously, these amperometric responses were attributed to the oxidation of thiocholine produced by the hydrolysis of ATCl, which were catalyzed by immobilized AChE. At the AChE/Au–Pd/IL-GR–CHI/GCE (curve e), the oxidation peak current was higher than that of the AChE/IL-GR–CHI/GCE (curve d). It indicated that Au–Pd could greatly improve electron transfer, thus increasing the peak current and the sensitivity of the biosensor.

3.4. The superiority of the Au–Pd/IL-GR–CHI/GCE

In order to evaluate the conductivity of different nanocomposites (IL-GR–CHI, Pd/IL-GR–CHI, Au/IL-GR–CHI and Au–Pd/IL-GR–CHI), four kinds of different modified GCEs were

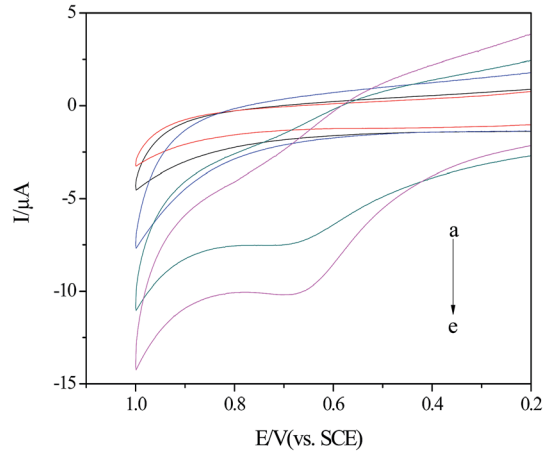

Fig. 3 Cyclic voltammogram of the GCE (a), AChE/Au–Pd/IL-GR–CHI/GCE (b) in 0.1 M PBS (pH 6.5) without ATCl and Au–Pd/IL-GR–CHI/GCE (c), AChE/IL-GR–CHI/GCE (d), and AChE/Au–Pd/IL-GR–CHI/GCE (e) in 0.1 M PBS (pH 6.5) containing 1.0 mM ATCl, scan rate 50 mV s^{-1}.

prepared. Fig. 4(A) shows the electrochemical impedance spectroscopy spectra of the respective modified GCE, and the equivalent electrical circuit used to fit the electrochemical impedance data is the same as in Fig. 2B. The observed R_{et} value of the IL-GR–CHI/GCE electrode was 188.5 Ω (curve a). When the electrodeposition of Pd (or Au) nanoparticles was performed on the IL-GR–CHI/GCE (curve b and curve c), the R_{et} value of the modified electrode was smaller than that of the IL-GR–CHI/GCE electrode, the reason may be due to the excellent conductivity of Pd (or Au) nanoparticles, which was beneficial for the electron transfer to take place. Moreover, when the IL-GR–CHI/GCE was covered by the electrodeposition of Au–Pd bimetallic nanoparticles (curve d), the smallest R_{et} value obtained owing to Au–Pd nanoparticles may act as a bridge of electron transfer and promote the electron transfer. The results showed that hybrid nanoparticles displayed superior electrochemical performance in comparison with that of nanoparticles alone.

To prove the advantage of the AChE/Au–Pd/IL-GR–CHI/GCE, DPV responses on different electrodes were also studied in pH 6.5 PBS containing 1.0 mM ATCl, and the results are shown in Fig. 4(B). It can be seen that the oxidation peaks appeared on the AChE/IL-GR–CHI/GCE (a), AChE/Pd/IL-GR–CHI/GCE (b), AChE/Au/IL-GR–CHI/GCE (c) and AChE/Au–Pd/IL-GR–CHI/GCE (d). Obviously, these peaks came from the oxidation of thiocholine, the hydrolysis product of ATCl, catalyzed by the immobilized AChE. The oxidation peak current of thiocholine was 1.88 μA at the AChE/IL-GR–CHI/GCE electrode (curve a). When the electrode was modified by the AChE/Pd/IL-GR–CHI/GCE (curve b) or the AChE/Au/IL-GR–CHI/GCE (curve c), the oxidation peak current of thiocholine was greater than that at the AChE/IL-GR–CHI/GCE, which indicated that Au or Pd nanoparticles could enhance the sensitivity of the biosensor in the detection of pesticides. Pd/IL-GR–CHI (or Au/IL-GR–CHI) nanocomposite-modified electrodes, possessing good conductivity and catalytic activity, could provide an extremely hydrophilic surface for AChE adhesion. As expected, the maximum oxidation peak current was obtained at the AChE/Au–Pd/IL-GR–CHI/GCE (curve d), which dramatically exceeded the current obtained at the AChE/Pd/IL-GR–CHI/GCE and the AChE/Au/IL-GR–CHI/GCE. The sharp increase could be attributed to the joint contribution of IL-GR and Au–Pd. The conductivity of IL-GR, the big surface area and the electrochemical catalytic properties of Au–Pd had a synergistic effect on promoting AChE adhesion, which led to the significant enhancement of the current response.

3.5. Optimization parameters of the biosensor performance

The effect of solution pH on the peak current response was studied in a series of PBS containing 1.0 mM ATCl with the pH from 6.0 to 8.5 by DPV. As shown in Fig. 5A, the maximum

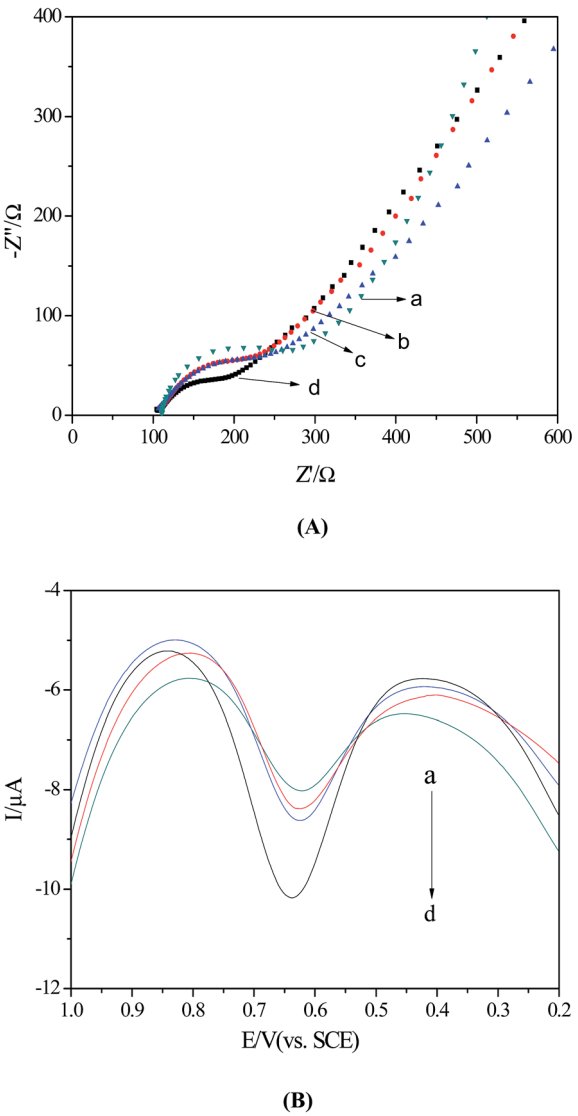

Fig. 4 (A) Electrochemical impedance spectroscopy spectra of the IL-GR–CHI/GCE (a), Pd/IL-GR–CHI/GCE (b), Au/IL-GR–CHI/GCE (c) and Au–Pd/IL-GR–CHI/GCE (d) in 5.0 mM $[Fe(CN)_6]^{3-/4-}$ containing 0.1 M KCl. (B) The differential pulse voltammogram of the AChE/IL-GR–CHI/GCE (a), AChE/Pd/IL-GR–CHI/GCE (b), AChE/Au/IL-GR–CHI/GCE (c) and AChE/Au–Pd/IL-GR–CHI/GCE (d) in 0.1 M PBS (pH 6.5) containing 1.0 mM ATCl.

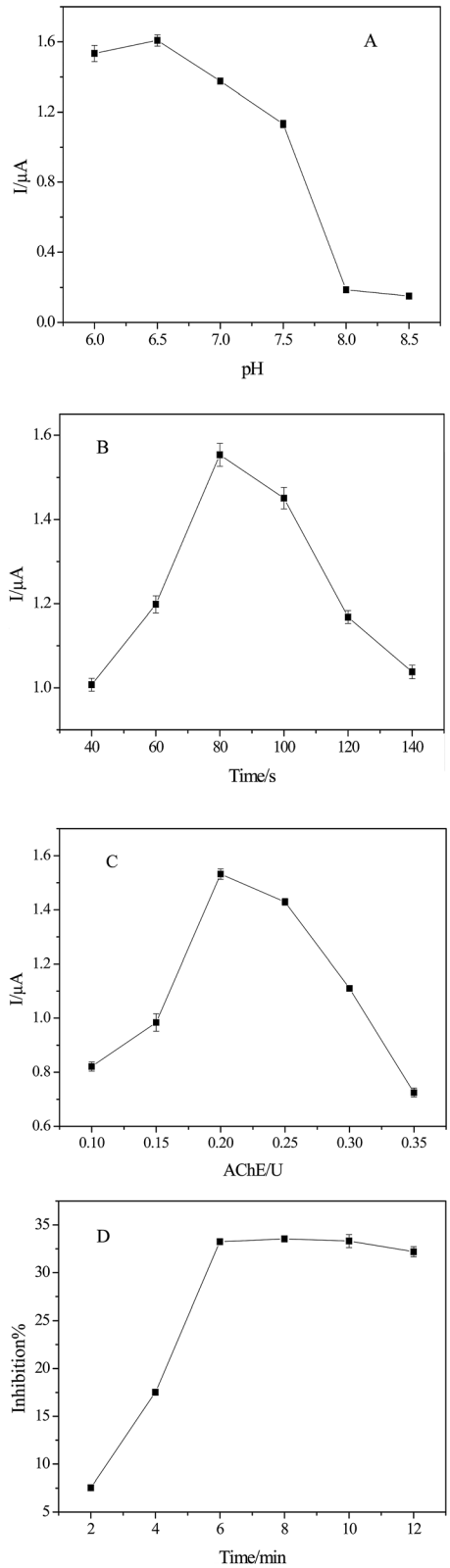

Fig. 5 Effect of pH (A), deposition time (B), AChE loading (C) and inhibition time (D) on the response of the biosensor.

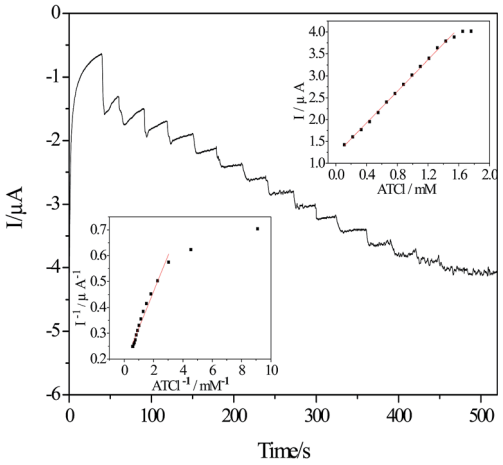

Fig. 6 Typical current–time plot for the biosensor on successive addition of ATCl to pH 6.5 PBS under stirring at an applied potential of 0.70 V. The inset shows the calibration plot for the ATCl sensor (upper right) and the reciprocal relationship between the ATCl concentration and the current response (bottom left).

response peak current appeared at pH 6.5. Therefore, pH 6.5 was selected in the detection solution.

It is reported that the deposition time can control the distribution of Au–Pd nanoparticles. The relationship between the peak current and the deposition time of Au–Pd nanoparticles was also investigated (Fig. 5B). With the deposition time from 40 s to 140 s, the response peak current increased and reached the maximum at 80 s. So we selected 80 s as the deposition time in this study.

Fig. 5C displays the effect of AChE loading on the biosensor response. It was noticed that the DPV peak current increased with increasing amount of AChE and reached the maximum at 0.2 U. Further increase of AChE led to an obvious decrease of

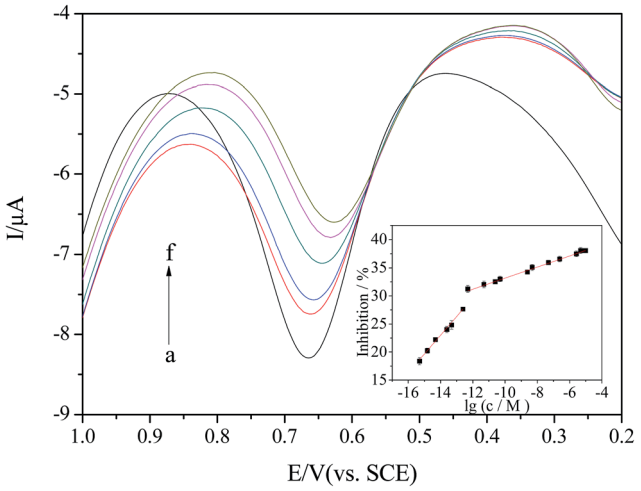

Fig. 7 The DPV (at 50 mV s^{-1}) of the AChE/Au–Pd/IL-GR–CHI/GCE biosensor in 0.1 M PBS (pH 6.5) containing 1.0 M ATCl after incubation in different concentrations of phorate (a–f: 0, 4.9×10^{-14}, 2.5×10^{-13}, 4.9×10^{-12}, 4.9×10^{-10}, and 4.8×10^{-8} M) for 6 min. The inset shows the inhibition of the AChE/Au–Pd/IL-GR–CHI/GCE biosensor *versus* the logarithm of the phorate concentration.

Table 1 Performance comparison with other reported biosensors for OP detection

Electrode material	Linear range (M)	Detection limit (M)	Analyte	Reference
AChE-nano$CaCO_3$-CS[a]/GCE	1.9×10^{-8}–7.5×10^{-7} and 2.8×10^{-6}–1.4×10^{-5}	3.8×10^{-9}	Methyl parathion	40
AChE/Au-PPy[b]-rGO[c]/GCE	1.0×10^{-9}–5.0×10^{-6}	5.0×10^{-10}	Paraoxon-ethyl	41
NF[d]/AChE-CS/Pt-CGR[e]-NF/GCE	1.0×10^{-12}–1.0×10^{-10} and 1.0×10^{-10}–1.0×10^{-8}	5.0×10^{-13}	Carbofuran	42
AChE/AgNPs-CGR-NF/GCE	1.0×10^{-12}–1.0×10^{-8}	5.5×10^{-13}	Carbaryl	43
NF/AChE-CS/ZnO-CGR-NF/GCE	1.0×10^{-13}–1.0×10^{-8}	5.0×10^{-14}	Chlorpyrifos	44
NF/AChE-CS/SnO_2-CGR-NF/GCE	1.0×10^{-13}–1.0×10^{-10} and 1.0×10^{-10}–1.0×10^{-8}	5.0×10^{-14}	Methyl parathion	45
AChE/Au–Pd/IL-GR–CHI/GCE	5.0×10^{-16}–2.5×10^{-13} and 4.9×10^{-13}–9.5×10^{-6}	2.5×10^{-16}	Phorate	This work

[a] Chitosan. [b] Polypyrrole. [c] Reduced graphene oxide. [d] Nafion. [e] Carboxylic graphene.

the current response. This may be due to the fact that the superabundant AChE possibly increased the electrode resistance of the modified electrode and was unstable. Thus, 0.2 U of AChE was chosen as the optimal enzyme concentration for the fabricated biosensor.

The effect of inhibition time on the biosensor response was also discussed. The AChE/Au–Pd/IL-GR–CHI/GCE biosensor was incubated in 1.0×10^{-9} M phorate standard solution for different periods of time. As shown in Fig. 5D, the inhibition rate showed an obvious increase with the increase of inhibition time within 6 min, however, when the inhibition time was longer than 6 min, there was no obvious increase, indicating an equilibration state. Thus, the optimum inhibition time of 6 min was used for the incubation steps in this study.

3.6. Detection of ATCl at the AChE/Au–Pd/IL-GR–CHI/GCE biosensor

Under the optimized experimental conditions, the AChE biosensor was explored by amperometric measurements. Fig. 6 shows a typical amperometric current–time response of the biosensor after the successive addition of ATCl to pH 6.5 PBS. As the inset of Fig. 6 shows, the current linearly increased with the increase of ATCl concentration over the range from 0.11 to 1.54 mM.

At higher ATCl concentrations, the shape of the amperometric response was indicative of a Michaelis–Menten process. The apparent Michaelis–Menten constant K_m^{app} of the biosensor was calculated to be 0.78 mM from the Lineweaver–Burk equation. The value was much lower than 1.75 mM obtained from the carbon nanotube modified electrode[38] and 1.5 mM obtained from the polyethyleneimine modified electrode,[39] indicating the good affinity of AChE to the substrate.

3.7. Detection of pesticides

After incubation of the biosensor with different concentrations of phorate, DPV responses of the biosensor were determined and are shown in Fig. 7. It shows that the peak currents (curves b–f) dramatically decreased compared with that of the control (curve a), and the decrease in peak current increased with the increasing concentration of phorate. The calibration plot of inhibition percentage (I%) *versus* phorate concentration is shown in the inset of Fig. 7. Linear equations of phorate were I (%) = 3.340 log c + 69.74 (r = 0.994) from 5.0×10^{-16} to 2.5×10^{-13} M and I (%) = 0.986 log c + 43.02 (r = 0.990) from 4.9×10^{-13} to 9.5×10^{-6} M, with a detection limit of 2.5×10^{-16} M ($S/N = 3$). The results indicated that the biosensor was more sensitive for detecting low concentrations of pesticides than high concentrations of pesticides.

The comparison between the performance of the proposed biosensor and other reported AChE biosensors in the literature is summarized in Table 1. Compared with the reported biosensors,[40–45] the AChE/Au–Pd/IL-GR–CHI/GCE showed a lower detection limit and wider linear range, which may be due to the exciting electronic properties of Au–Pd nanoparticles and the excellent bioactivity of IL-GR–CHI hybrids.

3.8. Interference study

The interfering signal due to the most common electroactive species was investigated in our experiment. The signal for 0.5 mM ATCl was compared with the signal obtained in the presence of the interfering species. The results showed that no noticeable changes in DPV responses were observed in the presence of Ca^{2+} (0.5 mM), Mg^{2+} (0.5 mM), Fe^{3+} (0.5 mM), SO_4^{2-} (0.5 mM), NO_3^- (0.5 mM), glucose (0.5 mM), citric acid (0.5 mM) and oxalic acid (0.5 mM). However, 0.5 mM of phenol, 0.5 mM of *p*-nitrophenol, 0.5 mM of *p*-nitroaniline and 0.5 mM of catechol severely interfered with the determination. In addition, the interference study of other OPs such as malathion (or parathion) was also discussed; the results indicated that equal concentrations of malathion (or parathion) and phorate interfered with each other for the determination.

3.9. Reproducibility and stability of the AChE/Au–Pd/IL-GR–CHI/GCE

The reproducibility of the AChE/Au–Pd/IL-GR–CHI/GCE biosensor was evaluated by analyzing phorate for six replicate measurements in 1.0 mM ATCl after being treated with

Table 2 Recovery of phorate in spiked apple juice samples (n = 3)

Sample	Added (M)	Found (M)	Recovery (%)	RSD (%)
1	5.0×10^{-13}	4.9×10^{-13}	98.0	3.4
2	5.0×10^{-12}	5.4×10^{-12}	108.0	2.8
3	1.0×10^{-10}	9.1×10^{-11}	91.0	3.2
4	5.0×10^{-8}	5.2×10^{-8}	104.0	2.9
5	1.0×10^{-7}	1.1×10^{-7}	110.0	3.8

2.0×10^{-10} M phorate for 6 min. Similarly, the inter-assay precision was estimated at five different electrodes for the determination. The coefficient of variation of intra-assay and inter-assay was 3.35% and 4.51%, respectively, which indicated that the AChE/Au–Pd/IL-GR–CHI/GCE biosensor was reproducible and precise. The prepared AChE/Au–Pd/IL-GR–CHI/GCE biosensor was stored at 4 °C when not in use. After a 15 day storage period, the biosensor retained 95.4% of its initial current response, proving the acceptable stability.

3.10. Analysis of phorate in spiked apple juice samples

Apple juices were spiked with varying concentrations of phorate as described in the Experimental section, and were measured to evaluate the reliability of the proposed AChE/Au–Pd/IL-GR–CHI/GCE biosensor. As shown in Table 2, the recoveries were found to be between 91.0% and 110.0% for phorate detection. The results indicated that the proposed biosensor is acceptably accurate and precise, and can be used for the analysis of samples from a real environment.

4. Conclusion

The present study demonstrates a new approach toward advanced development of a highly sensitive electrochemical assay of OPs by using Au–Pd bimetallic nanoparticles and the ionic liquid functionalized graphene–chitosan hybrid nanocomposite (Au–Pd/IL-GR–CHI) modified glassy carbon electrode. Using Au–Pd/IL-GR–CHI hybrid nanocomposites not only accelerated direct electron transfer from the enzyme to the electrode surface, but also enhanced the amount of AChE immobilized, which greatly improved the electrochemical properties of the biosensor interface. Moreover, the sensitivity of the biosensor could be enhanced greatly. The biosensor also demonstrated excellent stability. The satisfactory results obtained in apple juice sample analysis demonstrate that the biosensor has great potential for practical applications.

Acknowledgements

This research was supported by National Natural Science Foundation of China (no. 21275039).

References

1 E. Ballesteros and M. J. Parrado, *J. Chromatogr. A*, 2004, **1029**, 267–273.
2 X. Gao, G. C. Tang and X. G. Su, *Biosens. Bioelectron.*, 2012, **36**, 75–80.
3 X. Sun, Y. Zhu and X. Y. Wang, *Food Control*, 2012, **28**, 184–191.
4 P. Uutela, R. Reinila, P. Piepponen, R. A. Ketola and R. Kostiainen, *Mass Spectrom.*, 2005, **19**, 2950–2956.
5 D. Du, M. H. Wang, J. Cai and A. D. Zhang, *Sens. Actuators, B*, 2010, **146**, 337–341.
6 R. Rawal, S. Chawla, T. Dahiya and C. S. Pundir, *Anal. Bioanal. Chem.*, 2011, **401**, 2599–2608.
7 P. Raghu, T. Madhusudana Reddy, B. Kumara Swamy, B. Chandrashekar, K. Reddaiah and M. Sreedhar, *J. Electroanal. Chem.*, 2012, **665**, 76–82.
8 Z. Sun, D. K. James and J. M. Tour, *J. Phys. Chem. Lett.*, 2011, **2**, 2425–2432.
9 N. Liu, L. Fu, B. Dai, K. Yan, X. Liu, R. Q. Zhao, Y. F. Zhang and Z. F. Liu, *Nano Lett.*, 2011, **11**, 297–303.
10 X. L. Dong, J. S. Cheng, J. H. Li and Y. S. Wang, *Anal. Chem.*, 2010, **82**, 6208–6214.
11 F. W. Li, M. Q. Xue, X. L. Ma, M. N. Zhang and T. B. Cao, *Anal. Chem.*, 2011, **83**, 6426–6430.
12 M. Zhou, Y. M. Zhai and S. J. Dong, *Anal. Chem.*, 2009, **81**, 5603–5613.
13 S. Liu, J. Q. Tian, L. Wang, Y. L. Luo, W. B. Lu and X. P. Sun, *Biosens. Bioelectron.*, 2011, **26**, 4491–4496.
14 D. Chen, H. B. Feng and J. H. Li, *Chem. Rev.*, 2012, **112**, 6027–6053.
15 Y. Wang, S. Zhang, D. Du, Y. Y. Shao, Z. H. Li, J. Wang, M. H. Engelhard, J. H. Li and Y. H. Lin, *J. Mater. Chem.*, 2011, **21**, 5319–5325.
16 Y. Wang, Y. Y. Shao, D. W. Matson, J. H. Li and Y. H. Lin, *ACS Nano*, 2010, **4**, 1790–1798.
17 D. Li and R. B. Kaner, *Science*, 2008, **320**, 1170–1171.
18 J. M. Crosthwaite, S. N. V. K. Aki, E. J. Maginn and J. F. Brennecke, *J. Phys. Chem. B*, 2004, **108**, 5113–5119.
19 H. Ma and L. L. Dai, *Langmuir*, 2011, **27**, 508–512.
20 Q. Zhang, S. Y. Wu, L. Zhang, J. Lu, F. Verproot, Y. Liu, Z. Q. Xing, J. H. Li and X. M. Song, *Biosens. Bioelectron.*, 2011, **26**, 2632–2637.
21 D. Marquardt, C. Vollmer, R. Thomann, P. Steurer, R. Mülhaupt, E. Redel and C. Janiak, *Carbon*, 2011, **49**, 1326–1332.
22 C. S. Shan, H. F. Yang, D. X. Han, Q. X. Zhang, A. Ivaska and L. Niu, *Biosens. Bioelectron.*, 2011, **25**, 1504–1508.
23 R. Muszynski, B. Seger and P. V. Kamat, *J. Phys. Chem. C*, 2008, **112**, 5263–5266.
24 C. Xu, X. Wang and J. W. Zhu, *J. Phys. Chem. C*, 2008, **112**, 19841–19845.
25 A. P. Yu, P. Ramesh, M. E. Itkis, E. Bekyarova and R. C. Haddon, *J. Phys. Chem. C*, 2007, **111**, 7565–7569.
26 C. Z. Zhu, S. J. Guo, Y. M. Zhai and S. J. Dong, *Langmuir*, 2010, **26**, 7614–7618.
27 S. R. Cao, L. Zhang, Y. Q. Chai and R. Yuan, *Talanta*, 2013, **109**, 167–172.
28 R. Y. Wang, Z. W. Wu, C. M. Chen, Z. F. Qin, H. Q. Zhu, G. F. Wang, H. Wang, C. M. Wu, W. W. Dong, W. B. Fan and J. G. Wang, *Chem. Commun.*, 2013, **49**, 8250–8252.
29 R. Awasthi and R. N. Singh, *Carbon*, 2013, **51**, 282–289.
30 K. J. Chen, C. F. Lee, J. Rick, S. H. Wang, C. C. Liu and B. J. Hwang, *Biosens. Bioelectron.*, 2012, **33**, 75–81.
31 A. Safavi and F. Farjami, *Biosens. Bioelectron.*, 2011, **26**, 2547–2552.
32 X. H. Kang, Z. B. Mai, X. Y. Zou, P. X. Cai and J. Y. Mo, *Anal. Biochem.*, 2007, **369**, 71–79.
33 J. Liu, H. Q. Liu and L. Wang, *Appl. Organomet. Chem.*, 2010, **24**, 386–391.

34 H. F. Yang, C. S. Shan, F. H. Li, D. X. Han, Q. X. Zhang and L. Niu, *Chem. Commun.*, 2009, 3880–3882.
35 X. S. Guo, X. Y. Zhang, Q. Cai, T. Shen and S. M. Zhu, *Food Control*, 2013, **30**, 15–23.
36 J. Chai, F. Li, Y. Hu, Q. Zhang, D. Han and L. Niu, *J. Mater. Chem.*, 2011, **21**, 17922–17929.
37 M. E. Orazem and B. Tribollet, *Electrochemical impedance spectroscopy*, John Wiley & Sons, Inc., Hoboken, 2008.
38 G. Liu and Y. Lin, *Anal. Chem.*, 2006, **78**, 835–843.
39 D. Du, X. Ye, J. Cai, J. Liu and A. Zhang, *Biosens. Bioelectron.*, 2010, **25**, 2503–2508.
40 J. M. Gong, T. Liu, D. D. Song, X. B. Zhang and L. Z. Zhang, *Electrochem. Commun.*, 2009, **11**, 1873–1876.
41 Y. Q. Yang, A. M. Asiri, D. Du and Y. H. Liu, *Analyst*, 2014, **139**, 3055–3060.
42 L. Yang, G. C. Wang and Y. J. Liu, *Anal. Biochem.*, 2013, **437**, 144–149.
43 Y. J. Liu, G. C. Wang, C. P. Li, Q. Zhou, M. Wang and L. Yang, *Mater. Sci. Eng., C*, 2014, **35**, 253–258.
44 G. C. Wang, X. C. Tan, Q. Zhou, Y. J. Liu, M. Wang and L. Yang, *Sens. Actuators, B*, 2014, **190**, 730–736.
45 Q. Zhou, L. Yang, G. C. Wang and Y. Yang, *Biosens. Bioelectron.*, 2013, **49**, 25–31.